Electronic Supplementary Material (ESI) for Nanoscale.
This journal is © The Royal Society of Chemistry 2014

Electronic Supplementary Material (ESI) for

Sustainable Molecular Oxygen Activation with Oxygen Vacancies on the {001} Facets of BiOCl Nanosheets under Solar Light

*Hao Li, Jinggu Shi, Kun Zhao, and Lizhi Zhang**

Key Laboratory of Pesticide & Chemical Biology of Ministry of Education, Institute of Environmental Chemistry, College of Chemistry, Central China Normal University, Wuhan 430079, P. R. China

*Corresponding author: Email: zhanglz@mail.ccnu.edu.cn (L.Z. Zhang)

Preparation of photocatalyst.

I. For the preparation of BiOCl microsphere assembled by {001} facets exposed single crystalline nanosheets, x mmol (x = 0.5, 1, 2, and 3) $Bi(NO_3)\cdot5H_2O$ were added slowly into 16 mL ethylene glycol (EG) solution containing stoichiometric amounts of KCl. The mixture was stirred for 0.5 h at room temperature in air, and then poured into a 20 mL Teflon-lined stainless autoclave. The autoclave was allowed to be heated at 160 °C for 12 h under autogenous pressure, and then air cooled to room temperature. The resulting precipitates were collected and washed with deionized water and ethanol to remove the residual ions. The final product was dried at 60 °C in air for further use. The corresponding sample was designated as BOC-001-x (x = 0.5, 1, 2 and 3). For comparison, the counterpart sample without oxygen vacancies (OVs) confined on the {001} facets was synthesized by heating BOC-001-3 at 300 ^{o}C in the air for 4 h to reoxidize the surface and was denoted as BOC-001-H.

II. For the preparation of SiO_2 coated BOC-001-3, 0.2 g of BOC-001-3 was well dispersed in a mixture of 40 mL of ethanol and 10 mL of deionized water in an ultrasonic bath and stirred for 30 min at 40 ^oC. Then 1.5 mL of NH_4OH (25 wt %) was added to the dispersion. After that, 0.05 mL of tetraethyl or thosilicate was rapidly injected and the reaction continued for 2 h. The resultant sample (denoted as BOC-001-3-SiO_2) was centrifuged and washed thoroughly with water and absolute ethanol, and finally dried in air at 60 ^oC.

III. TiO_2 with {001} facets exposed (TiO_2-001) was prepared through the method reported by Han et al.[1] In a typical synthesis, 20 mL of $Ti(OBu)_4$ and 2 mL of hydrofluoric acid solution were mixed in 80 mL Teflon autoclave, and then kept at 180 ^oC for 24 h. After being cooled to room temperature, resultant TiO_2 was separated and washed with ethanol and distilled water for several times. Finally the white TiO_2 powder was annealed under 400 ^oC for 2 h in the air to remove the surface fluoride ions.

Ultra-high vacuum (UHV) was adopted to create OVs on the {001} facets of TiO_2 according to the method reported by Xing et al.[2] In a typical synthesis, 0.1 g TiO_2-001 was homogeneously spread in a crucible and then annealed at 200 ^oC for 2h in the vacuum condition with a heating rate of 5 ^oC/min. Resultant TiO_2 was denoted as TiO_2-001-OV.

Characterization. The powder X-ray diffraction (XRD) were recorded on a Rigaku D/MAX-RB diffractometer with monochromatized Cu Kα radiation (λ = 0.15418 nm). The scanning electron microscope (SEM) images and energy-dispersive X-ray spectrum (EDS) were obtained with a JEOL 6700-F field-emission scanning electron microscope. The transmission electron microscopy (HRTEM) images were obtained by JEOL JSM-2010 high-resolution transmission electron microscopy. UV-visible absorption spectra of the samples were obtained using a UV-visible spectrophotometer (UV-2550, Shimadzu, Japan). Electron paramagnetic resonance (EPR) spectra were conducted on a Bruker EMX EPR Spectrometer (Billerica, MA). X-ray photoelectron spectroscopy (XPS) was obtained with Perkin-Elmer PHI 5000C and all binding energies were calibrated by using the contaminant carbon (C1S = 284.6 eV) as a reference. Raman spectra were obtained by a confocal laser micro-Raman spectrometer (Thermo DXR Microscope, USA) with a 532 nm laser. Total organic carbon (TOC) content of the prepared NaPCP solution was determined by a Shimadzu TOC-V CPH analyzer.

Analytical methods. Concentration of $\bullet O_2^-$ was determined by its selective reaction with nitroblue tetrazolium (exhibiting an absorption maximum at 259 nm).[3] A (p-hydroxyphenyl) acetic acid (POHPAA) analysis method was used to detect the amount of generated H_2O_2. The reaction product of H_2O_2 with POHPAA fluorescence reagent had a strong fluorescent emission at 409 nm when excited at 315 nm.[4] As benzoic acid (BA) can react with •OH in a well-defined manner and obey the pseudo-first-order kinetics, the concentration of •OH was determined by employing the oxidation of BA as the model reaction.[5]

Theoretical calculation. All calculations were carried out using the density of functional theory (DFT) with the exchange-correlation functionals described by GGA-PBE.[6] (1×1) surface was used to test the thickness of the atomic layers of the slabs. The test was implemented by the CASTEP code, in which the plane-wave pseudopotential approach and ultrasoft pseudopotentials were employed for all the atoms with a kinetic energy cutoff of 380 eV.[7-8] During geometry optimization, the surface structure were relaxed to an energy convergence of 10^{-5} eV/atom and a force convergence of 0.03 eV/Å. A Monkhorst-Pack mesh for BiOCl with {001} facets exposed were 4 × 4 × 1.[9] In DOS calculations, the k-points increased to 4 × 4 × 1 for the supercell. The vacuum in all the models was kept at 20 Å.

Photocatalytic activity test. All photocatalytic activity experiments were conducted at ambient temperature using a 500 W Xenon lamp with two 420 nm cutoff filter as the light source. For the oxidation of sodium pentachlorophenate (NaPCP), 0.05 g of photocatalyst was added into 50 mL of 10 mg•L^{-1} aqueous solution in a container. The mixture was continuously stirred in the dark for 60 min to ensure an adsorption-desorption equilibrium before the lamp was turned on. Five milliliters of the solution was taken out each 1 h and after centrifuged to remove the photocatalyst, concentration was monitored by colorimetry with the Shimadzu UV-2550 UV-vis spectrometer. Active species trapping experiments were conducted by adding the corresponding scavenger (0.01 mol/L) to the mixture before the lamp was turned on. Active trapping experiment was conducted by adding different kinds of excess scavengers: tert-butyl alcohol (TBA) for •OH, p-benzoquinone for $•O_2^-$, $Na_2C_2O_4$ for holes, catalase for H_2O_2.

Photocurrent measurements. To prepare photoelectrodes, the photocatalysts were dispersed in chitosan solution to form a 10 mg·mL^{-1} solution. Then, 0.3 mL of colloidal solution was dip-coated on the pretreated ITO surface and was allowed to dry under vacuum conditions for 24 h at room temperature. Photocurrent measurement was conducted on CHI660D Instruments in a standard three-electrode system with the BiOCl as the working electrode, Pt foil as the counter electrode, saturated calomel electrode as the reference electrode and 0.5 mol/L Na_2SO_4 aqueous solution as the electrolyte. Before the photocurrent measurement, Ar gas was purged into the Na_2SO_4 aqueous solution to remove the dissolved molecular oxygen for 30 min and kept purging during the photocurrent measurement. A LED light (UVEC-4II, Shenzhen Lamplic Technology Co. Ltd. China) with light intensity of 2000 mW/cm^2 was utilized as a monochromatic light source.

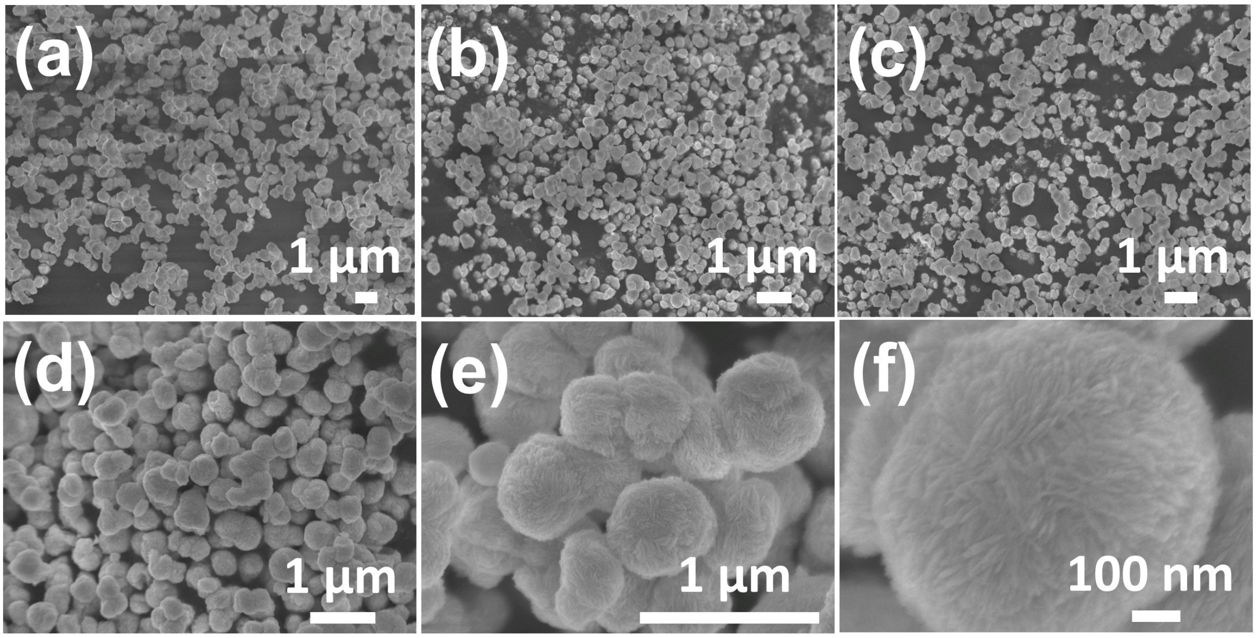

Figure S1. SEM images of (a) BOC-001-H, (b) BOC-001-0.5, (c) BOC-001-1 and (d) BOC-001-2. (e), (f) SEM images of BOC-001-3.

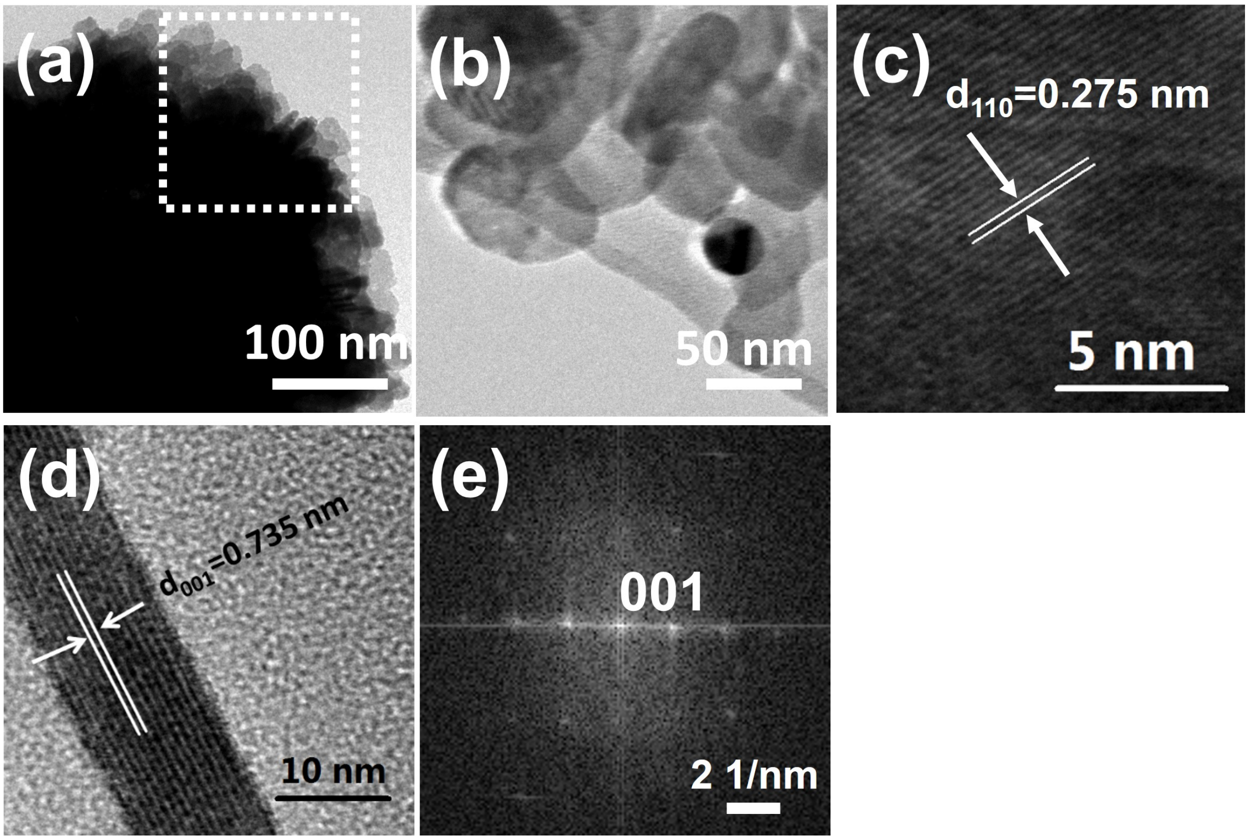

Figure S2. (a), (b) TEM images of the BOC-001-3 microsphere and (c-e) the corresponding HRTEM and FFT pattern of the nanosheets.

As revealed by SEM, BOC-001-x all consisted of microspheres with diameters of 0.5~1.0 μm assembled by radically grown nanosheets with thickness about 10 nm (Figure S1). TEM images further confirmed that the microsphere was densely constructed by single-crystalline nanosheets and HRTEM revealed the nanosheets as the building block is of fine crystallinity (Fiugre S2a-d). The lattice fringes with an interplanar lattice spacing of 0.275 nm was indexed as the (110) atomic plane (Figure S2c), while the lattice fringe spacing of 0.73 nm on the HRTEM image of a vertical nanosheet was assigned to the (001) plane of BiOCl (Figure S2d). Furthermore, the corresponding fast Fourier transform (FFT) pattern revealed that the single-crystalline nanosheet was indeed enclosed by dominant {001} facets (Figure S2e). Besides, percentage of {001} facets could be as high as 86%.

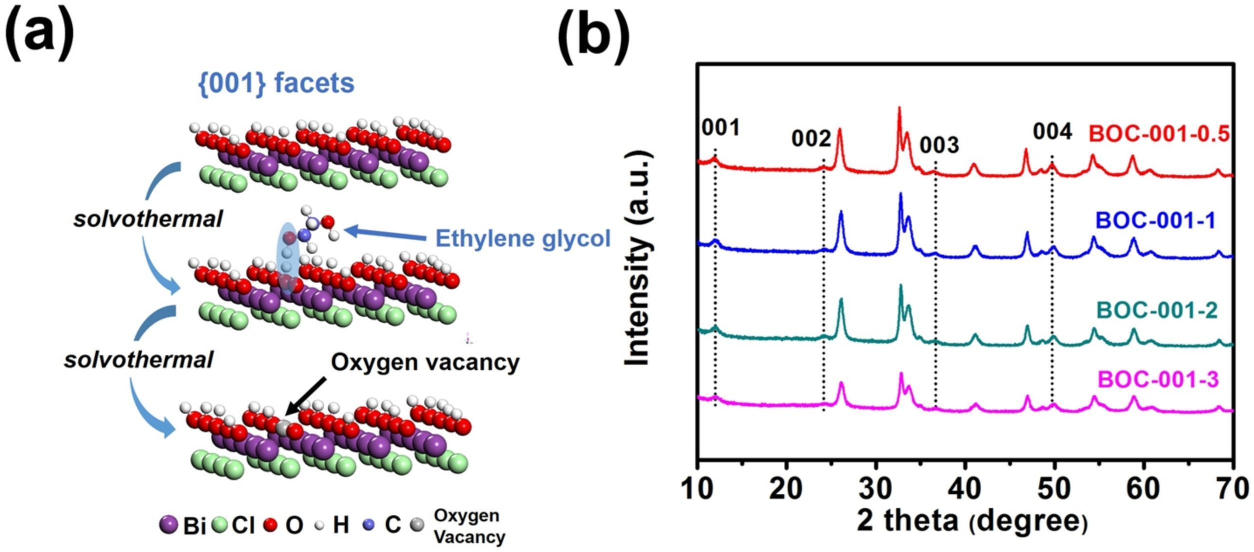

Figure S3. (a) Schematic illustration of the OVs generation on {001} facets of BiOCl during solvothermal synthesis. (b) XRD pattern of the as-prepared BiOCl photocatalysts.

OVs can be confined on the {001} facets through the redox reaction of {001} facets of BiOCl and EG during solvothermal synthesis, in which ethylene glycol molecules are evidenced to extract lattice oxygen atoms and leave OVs on the {001} facets (Figure S3).[10-11] Apart from that the as-prepared BiOCl could be readily indexed to the tetragonal phase of BiOCl [space group: *P4/nmm* (129), JCPDS file no. 73-2060], BOC-001-x gradually exhibited decreased diffraction peak intensity, indicating the crystallinity decrease with increase the bismuth precursor. Curiously, the (00L) related planes (L=1, 2, 3 and 4) suffered from serious weakened intensity, even though the BiOCl nanosheets were {001} facets exposed (Figure S3b). According to our previous studies, {001} facets exposure model of BiOCl is supposed to enhance relative intensity of the (00x) peak due to the highly preferred (00x) orientation in the nanosheets.[12] Therefore, we believed the possible reason accounting for the reduced (00x) peaks was arisen from defects on the {001} facets that seriously deteriorated the diffraction of X-ray on such facets.

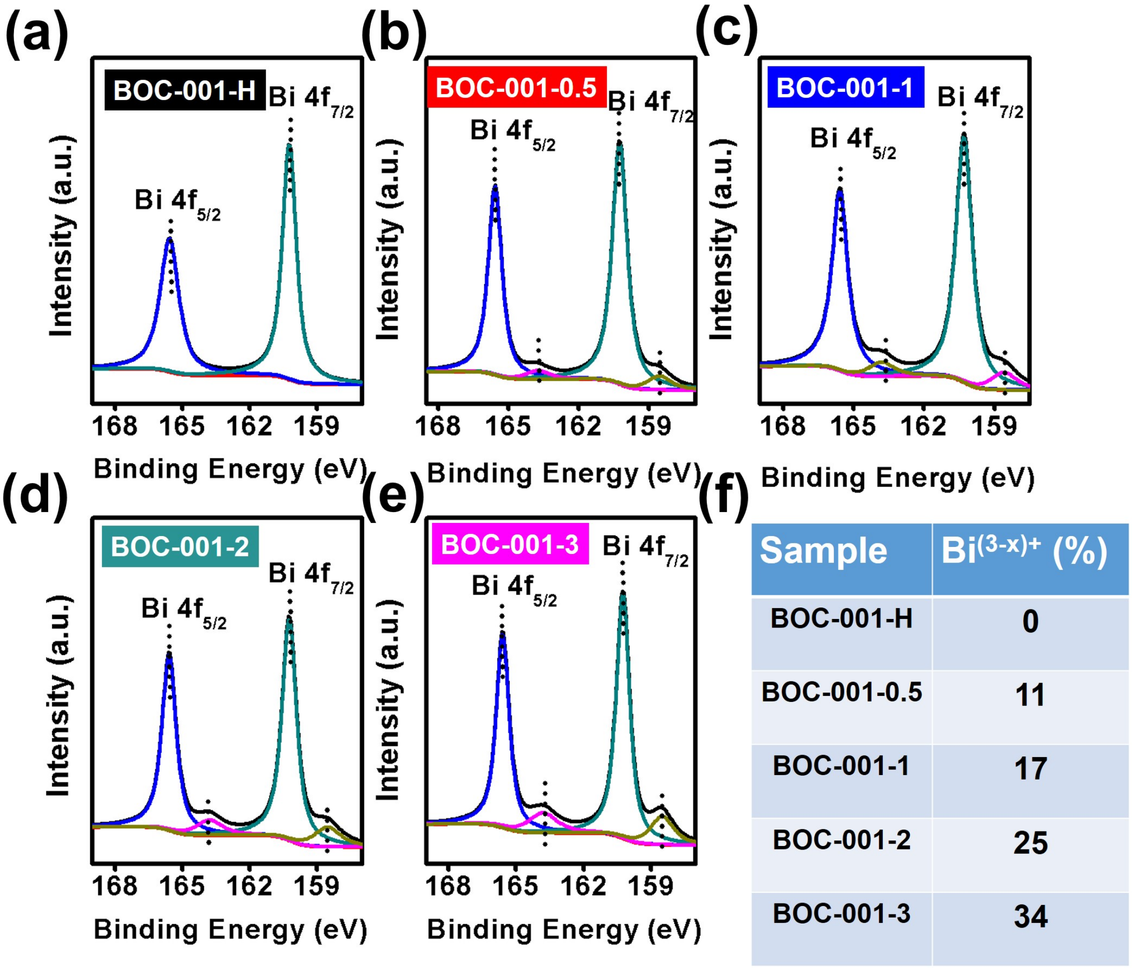

Sample	Bi$^{(3-x)+}$ (%)
BOC-001-H	0
BOC-001-0.5	11
BOC-001-1	17
BOC-001-2	25
BOC-001-3	34

Figure S4. High-resolution Bi 4f XPS spectra of (a) BOC-001-H, (b) BOC-001-0.5, (c) BOC-001-1, (d) BOC-001-2 and (e) BOC-001-3. (f) Percentages of Bi$^{(3-x)+}$ in the as-prepared BiOCl.

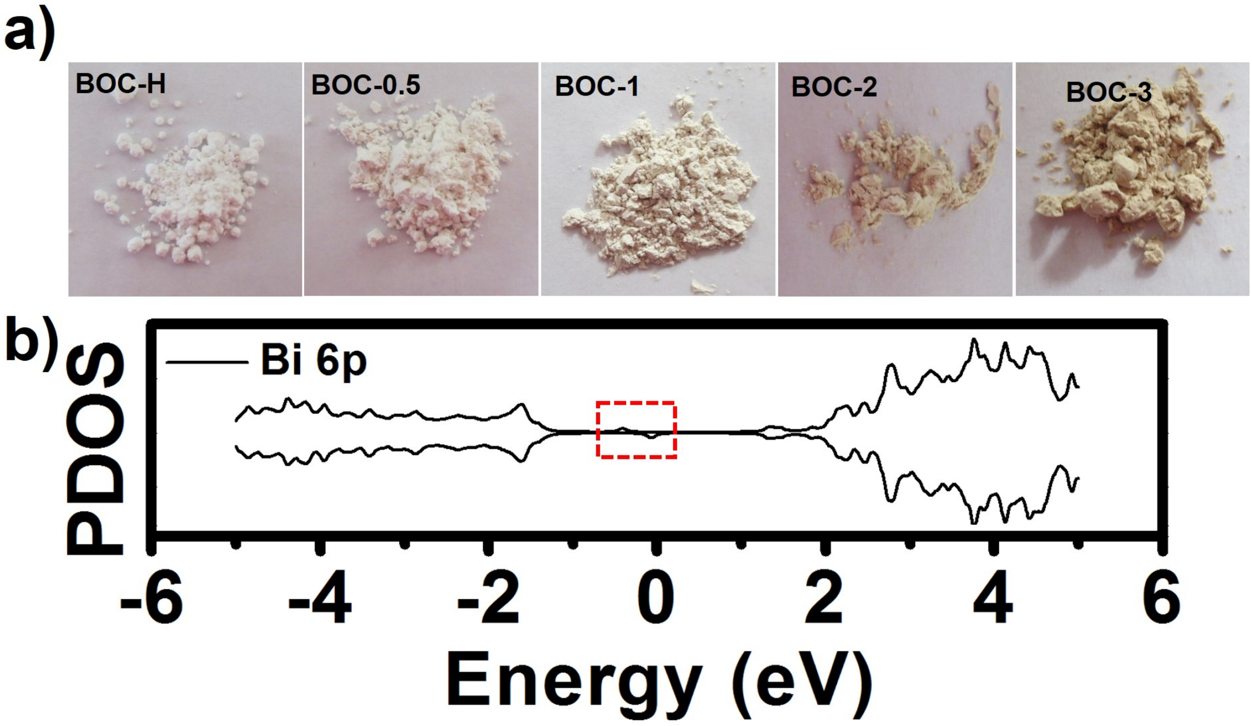

Figure S5. (a) Colors of the as-prepared BiOCl photocatalysts. (b) The partial density of states for the oxygen-deficient {001} facet (the dotted box showed the defect states contributed by Bi 6p state).

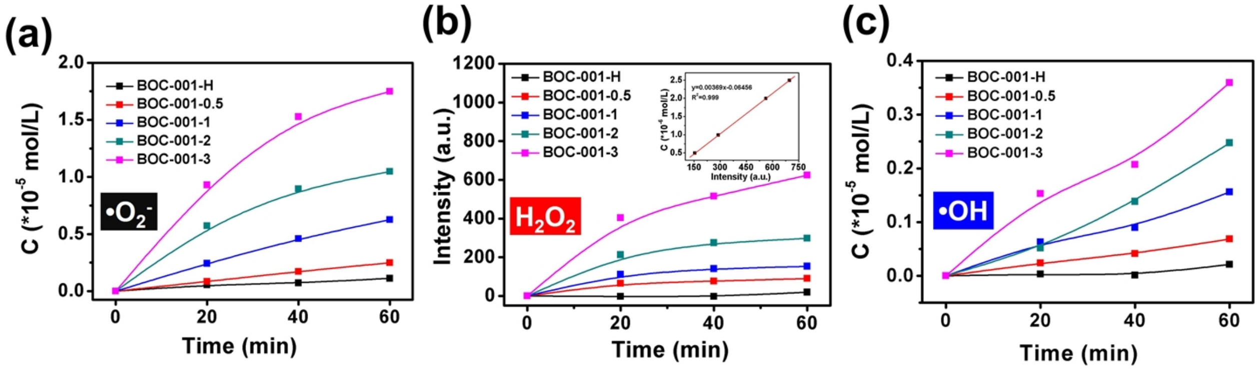

Figure S6. Quantitative determination of •O^{2-}, H_2O_2 and •OH over the as-prepared BiOCl. Error bar presented in Figure 3b and 3c were obtained by repeated the measurement of the above ROS for five times.

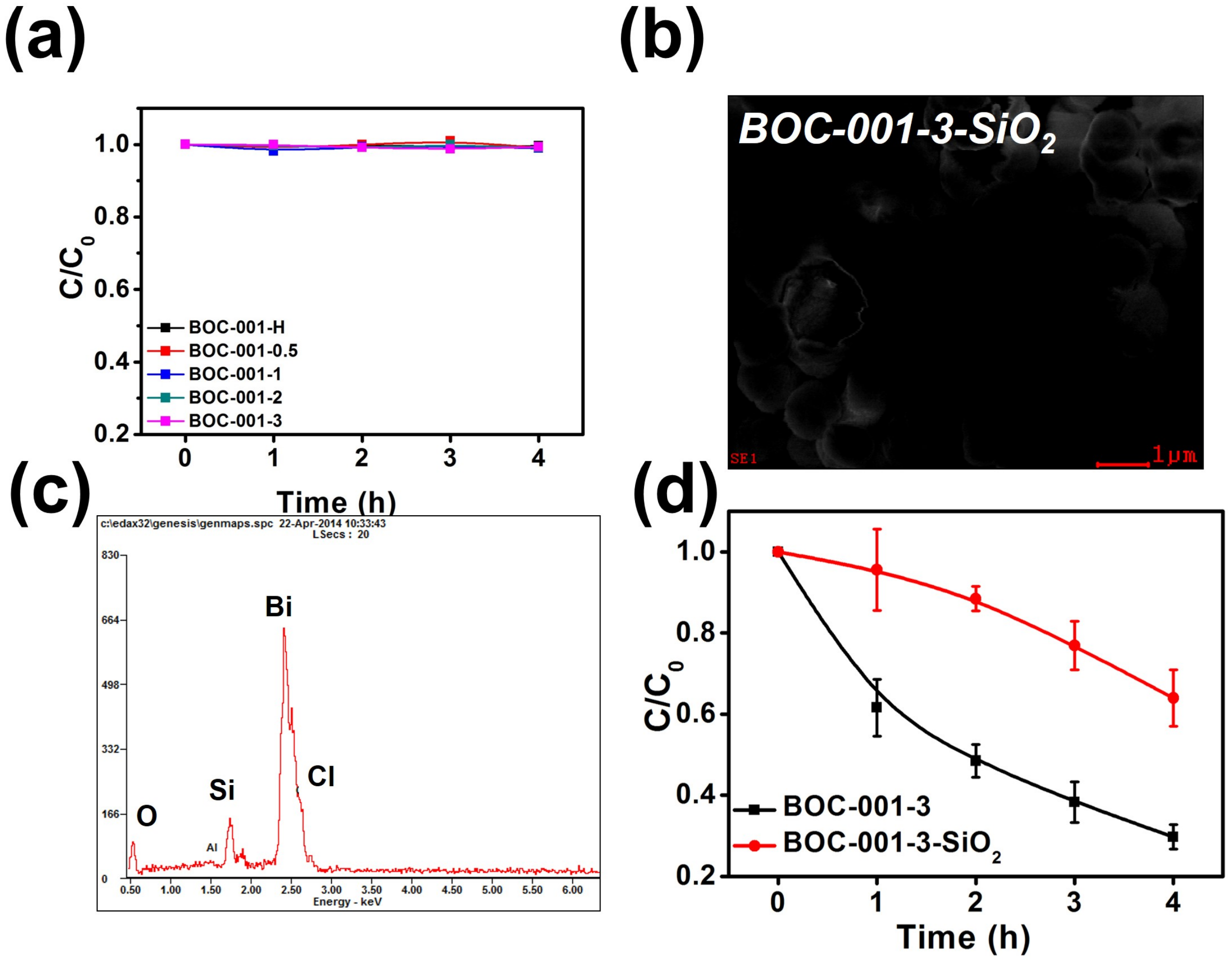

Figure S7. (a) The as-prepared BOC-001-x for the removal of NaPCP in the dark. (b), (c) SEM image of BOC-001-3-SiO_2 and the corresponding EDS spectra. (d) Photocatalytic removal of NaPCP over BOC-001-3 and BOC-001-3-SiO_2 under visible light.

Figure S7a revealed that the as-prepared BiOCl photocatalysts exhibited no activity for the degradation of NaPCP without light irradiation. Figure S7b is the SEM image of BOC-001-3-SiO_2 sprayed by carbon before characterization, which showed the presence of element Si signal according to the EDS spectra.

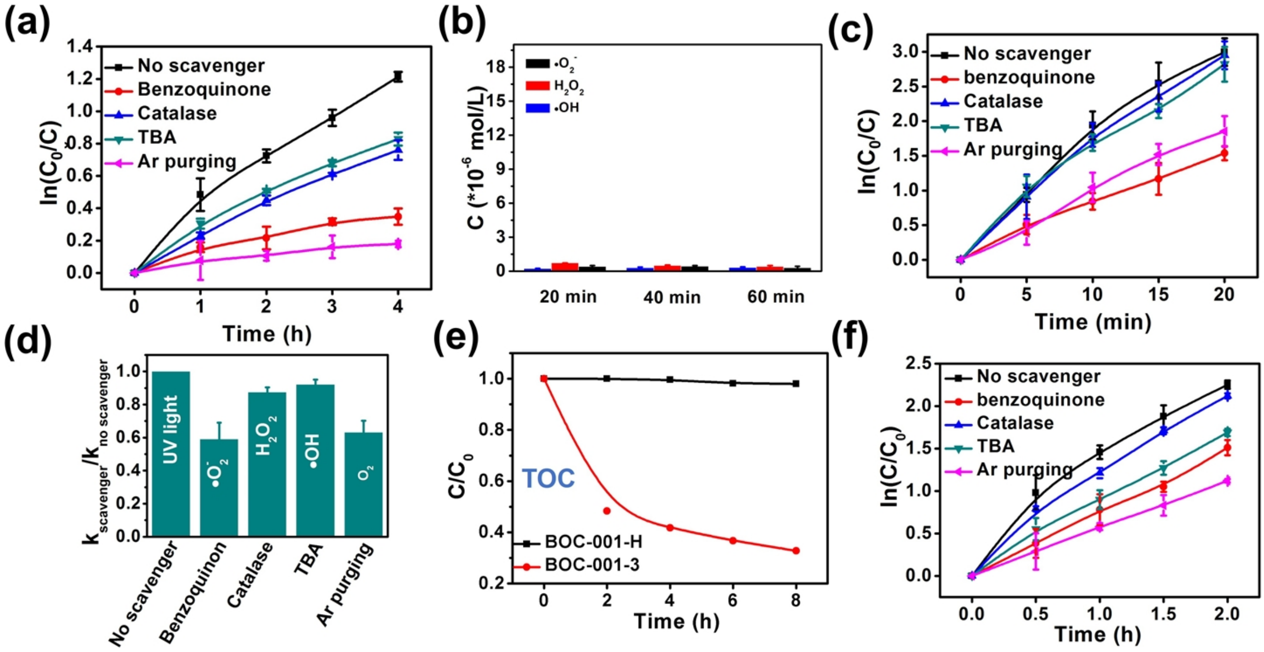

Figure S8. (a) Photocatalytic removal of NaPCP in the presence of different scavengers over BOC-001-3 under visible light. (b) ROS detected under visible light over BOC-001-3 when water-dissolved O_2 was removed. (c, d) Photocatalytic removal of NaPCP in the presence of different scavengers over BOC-001-3 under UV light. (e) The TOC change for the removal of NaPCP over BOC-001-3 under visible light. (f) Photocatalytic removal of NaPCP in the presence of different scavengers over BOC-001-3 under solar light.

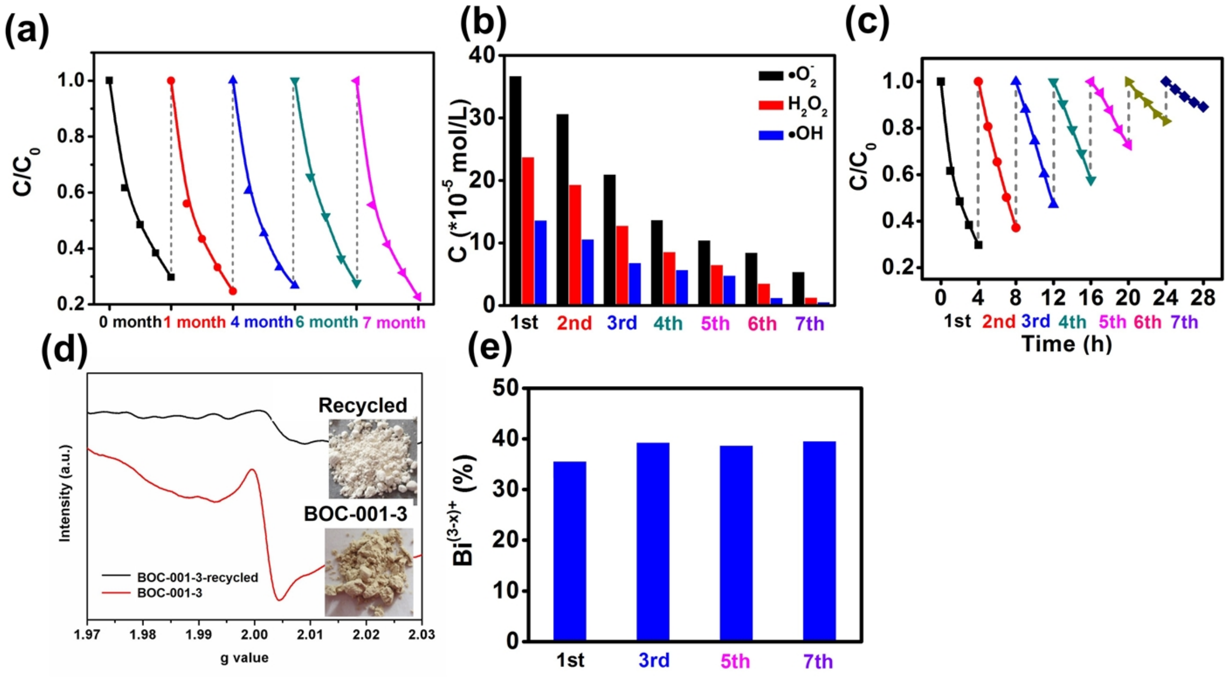

Figure S9. (a) Removal of NaPCP over BOC-001-3 under visible light after BOC-001-3 was stored in the dark for different months. Multi-cycle ROS generation (b) and photocatalytic NaPCP removal (c) with BOC-001-3 under visible light. (d) EPR spectra and color of the BOC-001-3 sample before and after repeated use under visible light. (e) Percentage of Bi$^{(3-x)+}$ in BOC-001-3 during repeated use under solar light.

After being used for 7 times, yellowish-brown BOC-001-3 became light-grey with a significant quenched OVs signal, indicating OVs were significantly healed via molecular oxygen dissociation under visible light (Figure S9d).

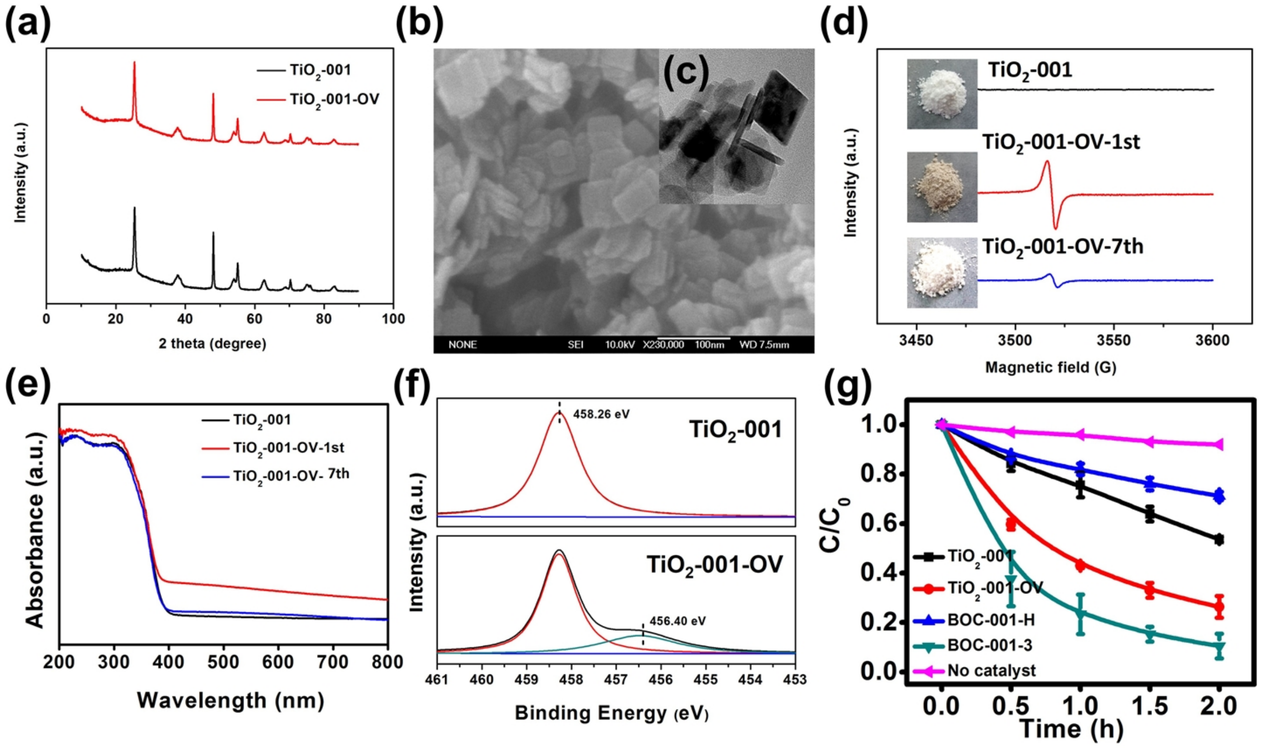

Figure S10. (a) XRD pattern of the as-prepared TiO_2. (b) SEM and (c) TEM images of TiO_2-001-OV. (d) EPR and (e) UV-vis absorption spectra of TiO_2-001-OV before and after repeated use. (f) XPS spectra of the as-prepared TiO_2. (g) Photocatalytic NaPCP removal in the absence or presence of the as-prepared TiO_2 and BiOCl photocatalysts under solar light.

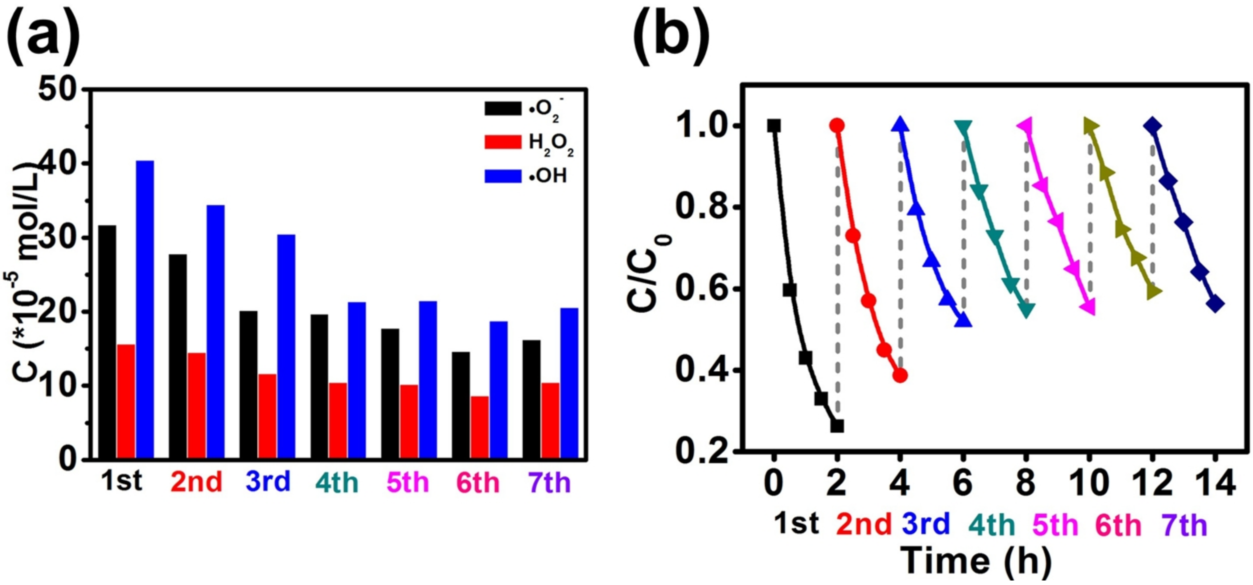

Figure S11. Multi-cycle ROS generation (a) and photocatalytic NaPCP removal (b) with TiO_2-001-OV under solar light.

XRD pattern revealed both TiO_2-001 and TiO_2-001-OV were of anatase phase (JCPDS No. 21-1272) and exhibited similar crystallinity (Figure S10a). As revealed by SEM and TEM images, the as prepared TiO_2 was of sheet-shaped structure with a typical {001} facets exposure model (Figure S10b and S10c). After the thermal treatment, white-colored TiO_2 became earth yellow, with a typical EPR signal and an absorption tail in the visible light region matching the features OVs (Figure S10d and S10e). Besides, emergence of binding energy at 456.4 eV was the characteristic feature of Ti^{3+}.[13-14] Moreover, the percentage of Ti^{3+} can be estimated by the peak area to be 33%, comparable to the percentage of $Bi^{(3-x)+}$ in BOC-001-3 (Figure S10f). Compared with TiO_2-001, TiO_2-001-OV exhibited notably enhanced photoreactivity for the degradation of NaPCP under solar light (Figure S10g). However, after multi-cycle ROS generation and photocatalytic NaPCP removal under solar light, color of TiO_2-001-OV changed to pale grey, with a quenched EPR signal and decreased absorption in visible light region (Figure S10d and S10e). These results indicated that OVs can be also healed through molecular oxygen dissociation under solar light. Under solar light, the self-degradation of NaPCP was 8%, which was negligible in comparison with the photocatalytic decomposition of NaPCP over BOC-001-3 (89.5 %) and TiO_2-001-OV (73.7%) under solar light

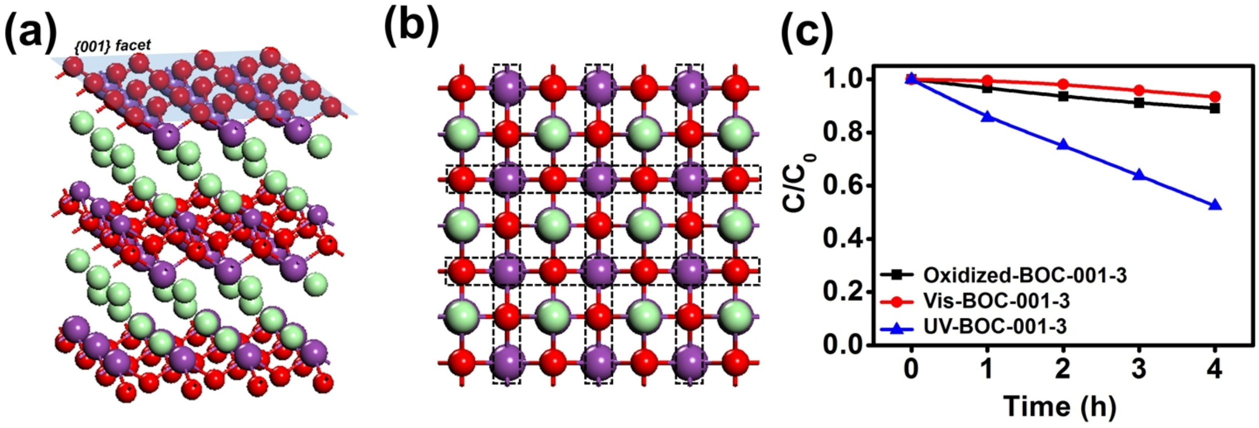

Figure S12. Side (a) and top (b) view of the {001} facet of BiOCl (the dotted boxes showed the crossed bridging rows with low-coordinated and closely interacted O atoms). (c) Photocatalytic removal of NaPCP under visible light with Oxidized-BOC-001-3 and visible & UV light-treated Oxidized-BOC-001-3.

To demonstrate that the refreshing effect was arisen from the UV irradiation, BOC-001-3 after the 7th cycle of NaPCP degradation under visible light (oxidized-BOC-001-3) was firstly irradiated under visible for 30 min in distilled water to obtain Vis-BOC-001-3. This Vis-BOC-001-3 photocatalyst showed slight decrease on the photocatalytic removal of NaPCP under visible light. As expected, 30 min's UV light irradiation of oxidized-BOC-001-3 could significantly enhance the photoreactivity of the obtained UV-BOC-001-3 for the NaPCP removal (Figure S12c).

Table S1 Physical properties and photocatalytic activity of the samples.

Sample	Average thickness (nm)	A_{BET} ($m^2\ g^{-1}$)	Kinetic constant (h^{-1})
BOC-001-3	9.7	25.8	1.08
TiO_2-001-OV	10.6	85.3	0.65

References

(1) Han, X.; Kuang, Q.; Jin, M.; Xie, Z.; Zheng, L. *J. Am. Chem. Soc.* **2009**, *131*, 3152.

(2) Xing, M. Y.; Zhang, J. L.; Chen, F.; Tian, B. Z. *Chem. Commun.* **2011**, *47*, 4947.

(3) (a) Blelskl, B. H.; Shlue, G. G.; Bajuk, S. *J. Phys. Chem.* **1980**, *84*, 830. (b) Xu, X. L.; Duan, X.; Yi, Z. G.; Zhou, Z. W.; Fan, X. M.; Wang, Y. *Catal.Commun.* **2010**, *12*, 169.

(4) Lazrus, A. L.; Kok, G. L.; Gitlin, S. N.; Lind, J. A.; McLaren, S. E. *Anal. Chem.* **1985**, 57, 917.

(5) Hirakawa, T.; Nosaka, Y. *Langmuir*, **2002**, *18*, 3247.

(6) Perdew, J. P.; Burke, K.; Ernzerhof, M. *Phys. Rev. Lett.* **1996**, *77*, 3865.

(7) Segall, M. D.; Lindan P. L. D.; Probert. M. J.; Pickard. C. J.; Hasnip, P. J.; Clark, S. J.; Payne, M. C. *J. Phys.: Cond. Matt.* **2002**, *14*, 2717.

(8) Vanderbilt, D. *Phys. Rev. B* **1990**, *41*, 7892.

(9) Monkhorst, H. J.; Pack, J. D. *Phys. Rev. B* **1976**, *13*, 5188.

(10) Jiang, J.; Zhang, L. Z.; Li, H.; He, W. W.; Yin, J. J. *Nanoscale* **2013**, *5*, 10573.

(11) Li, H.; Zhang, L. Z. *Nanoscale* **2014**, *6*, 7805.

(12) Jiang, J.; Zhao, K.; Xiao, X. Y.; Zhang, L. Z. *J. Am. Chem. Soc.* **2012**, *134*, 4473.

(13) Chen, X.; Burda, C. *J. Am. Chem. Soc.* **2008**, *130*, 5018.

(14) Asahi, R.; Morikawa, T.; Ohwaki, T.; Aoki, K.; Taga, Y. *Science* **2001**, *293*, 269.